Clays and Clay Minerals, Vol. 47, No. 3, 241–251, 1999.

CLAY MINERALOGY AND OCCURRENCE OF FERRIAN SMECTITES BETWEEN SERPENTINITE SAPROLITES AND BASALTS IN BIGA PENINSULA, NORTHWEST TURKEY

Ö. IŞIK ECE,[1] FAZLI ÇOBAN,[1] NURFER GÜNGÖR,[2] AND FİKRET SUNER[1]

[1] Istanbul Technical University, Mining Faculty, Mineralogy-Petrography Division, Maslak 80626 Istanbul, Turkey

[2] Science and Literature Faculty, Department of Physics, Maslak 80626 Istanbul, Turkey

Abstract—The clay mineralogy of an oxisol-saprolite overlying serpentinite and underlying basalt was studied with different techniques to evaluate the clay mineral transformation that occurred and to understand the origin of Fe^{3+}-rich smectite. The saprolite zone of the oxisol, up to 30 m thick, contains smectites of the montmorillonite-beidellite and montmorillonite-nontronite series, as well as illite, chlorite, talc, and goethite or amorphous oxyhydrates. Illite is mainly concentrated in the upper 50 cm thick zone underlying the basalt layer and chlorite-content increases toward altered serpentinite at the base. Minor amounts of nontronite formed mostly toward westward exposures where the hot contact layer between serpentinite and basalt is only 20 cm thick. Greene-Kelly Li-tests revealed that all samples contain montmorillonite, but one sample shows the presence of a minor amount of beidellite.

Parent rocks are a mixture of mainly mica schist (the source of beidellite), and minor serpentinite in different percentages and laterally distributed. These rocks were intensely weathered under humid climatic conditions. Silica was concentrated as amorphous transparent (pure silica) cobbles and milky quartz pebbles, and originated from geothermal solutions rising through the Ovacık thrust fault. The Mg partly formed chlorite. Ferrian smectites in serpentinites were derived obviously from the Mg-rich minerals but Mg is lost much more rapidly than Si during the formation of the clay deposit. The structural formula of the most Fe-rich smectite samples from the study area is $(Si_{6.60\text{-}7.10}\ Al_{1.40\text{-}0.90})(Al_{2.54\text{-}1.22}Mg_{0.32\text{-}0.92}Fe^{3+}{}_{1.18\text{-}1.68}Ti_{0.06\text{-}0.04})(Ca_{0.16\text{-}0.10}Na_{0.02}K_{0.02\text{-}\ 0.12})O_{20}(OH)_4$. This composition is within the range recorded for the ferrian montmorillonite-beidellite series, with very little vermiculite forming the oxisol-vertisol horizon.

Key Words—Alteration, Basalt, Beidellite, Ferric Iron, Mica Schist, Montmorillonite, Serpentinite, Turkey.

INTRODUCTION

The objective of this paper is to investigate the geologic setting of the study area, to examine the relationship between a thrust fault and clay occurrences, to document parent-rock alteration, and also to identify and characterize the occurrence of Fe-rich smectite minerals formed below Upper Miocene basalt lavas and overlying Permo-Triassic serpentinites. To better understand the genesis of the ferrian smectite series, it was necessary to map the study area in detail and to document stratigraphic features and clay mineral assemblages.

Present-day Fe^{3+}-beidellite and nontronite occurrences in deep ocean floors can be used as a possible analogue of Derbendbaşı-Kemerdere Fe^{3+}-smectite deposits in this study area. In contrast to hydrothermal veins in deep-sea spreading axes, Upper Miocene calc-alkaline basalt lavas (1000–1500°C) in the study area provided the necessary heat source for the transformation of Fe^{2+} to Fe^{3+} under strong oxidizing conditions during clay deposition. Si- and Fe-rich hydrothermal solutions were ascending from the thrust fault between the serpentinites and metamorphics-rock boundary.

Sherman *et al.* (1962) described the occurrences of nontronite and nontronite-like minerals in soils from weathered basalts and found that alteration is related to both the mode of occurrence of the parent rocks and the climatic (semi-arid, moderate rainfall, and humid tropical rainforest) and weathering environments. Intermediate members between nontronite and Fe-rich saponite were found in the Miocene Mariyama volcanic rocks, Gojome, Akita Prefecture, Japan, whereas nontronite is a product of leaching of trioctahedral iron-rich saponite by chemical weathering (Kimbara and Honda, 1975). The occurrence of nontronite veins has also been observed as an alteration product of volcanoclastic rocks in the Milos bentonites, Aegean Island, by Christidis *et al.* (1995).

The occurrence of ferruginous (Fe^{2+}) smectite minerals as alteration products of basic igneous rocks was reported by Miyamoto (1957), Sherman *et al.* (1962), and Delvigne *et al.* (1979). Clement and De Kimpe (1977) and Kodama and De Kimpe (1983) reported a nontronitic smectite, both ferruginous and magnesian, as the major secondary mineral in the clay-size fraction of a saprolite developed on gabbro. Kohyama *et al.* (1973) also studied iron-rich saponite derived from rhyolitic glassy tuffs and the existence of saponites rich in

ferrous (Fe^{2+}) and ferric (Fe^{3+}) iron by assuming a ferrous analogue of saponite as an end-member. Kodama *et al.* (1988) reported that this hypothesis appears to be particularly applicable to smectites rich in Mg and Fe, such as the ferruginous smectite found in the Mount Megantic gabbroic saprolite. Re-examination of a nontronite-like smectite from Mount Megantic indicates that it consists largely of a ferrian ($Fe^{3+} > Fe^{2+}$) smectite-like mineral with a small amount of a vermiculite-like mineral. The major component has a high substitution of Si by Al in the tetrahedral sheet and an excess charge in the octahedral sheet, as indicated by the chemical formula $(Mg_{1.14})(Mg_{1.15}Fe^{3+}_{1.05}Al_{0.28}Fe^{2+}_{0.17}Mn^{2+}_{0.04})(Si_{3.02}Al_{0.98})O_{10}(OH)_2$ (Kodama and De Kimpe, 1983).

The occurrence of an Fe^{3+}-rich montmorillonite-beidellite series was reported as the product of fault-related hydrothermal alteration of Miocene andesitic and trachyandesitic rocks in Biga peninsula, 40 km south of the study area (Çoban and Ece, 1999). Iron-rich, high-charge beidellites in soils were reported as a product of mica weathering and also formed from K-feldspar. During weathering, soil mica is transformed first to a vermiculite then to a beidellite, preserving the tetrahedral character of the charge (Badraoui *et al.* 1987; Badraoui and Bloom, 1990). Decarreau *et al.* (1987) synthesized a pure dioctahedral smectite from silico-ferric co-precipitates ($Si_4Fe^{3+}_{1.83}O_{10}(OH)_2Ca_{0.26}$), at temperatures of 100–150°C. Brigatti (1983) investigated chemical and crystallographic properties of natural dioctahedral Fe-rich smectites formed by weathering of basaltic rocks in the Bereci-Euganei, northern Italy. She found that the *b*-dimension could be correlated both to Fe^{3+}/Σ ratio (Σ = octahedral occupancy) and to dehydroxylation peak temperatures in the range 400–600°C; total octahedral occupancy is $\neq 2$ for dioctahedral smectites and in the smectite group there is not a continuous isomorphous series.

GEOLOGIC SETTING

The study area is located 40 km south of Çanakkale city, east of Dardanelles Strait (Figure 1). Four distinct NE-SW trending geotectonic zones are in the Biga and Gelibolu peninsulas, in the vicinity of Dardanelles Strait: the Gelibolu; the Ezine, which includes the study area; the Ayvacık-Karabiga; and the Sakarya zones (Okay *et al.*, 1990). The Ezine zone consists of a slightly metamorphosed epicontinental Permo-Carboniferous sedimentary sequence (the Karadağ unit) which is tectonically overlain by a Permo-Triassic ophiolite (the Denizgören ophiolite); both were thrust later over the high-grade metasedimentary rocks, mostly Permo-Carboniferous mica schists (Çamlıca metamorphics) (Okay *et al.*, 1990). The Ezine zone consists of the Çamköy thrust to the west, between the Karadağ unit (metaclastic, carbonate, flysch) and serpentinites, which are made mostly of harzburgite, and the Ovacık thrust to the east, between serpentinites and the Çamlıca mica schists. All Fe-rich smectites occur along the Ovacık thrust between the Derbendbaşı and Kemerdere areas (Figure 1).

Intense regional uplift at the end of Oligocene allowed all Middle-Eocene-Oligocene stratigraphic successions in the Biga peninsula to eroded almost completely, supplying the nearby basins with terrigenous, lacustrine, and very shallow marine sediments (Siyako *et al.*, 1989). These sedimentation sequences were covered by time-equivalent (Early-Middle Miocene) calc-alkaline volcanic rocks (andesitic, dasitic, rhyodasitic and latitic lavas, acidic tuffs, aglomerates, and ignimbrites) while several large granodiorite plutons were emplaced during this period. These calc-alkaline basalts in the study area are the product of Upper Miocene volcanism (Ercan *et al.*, 1995).

The upper layers of the Çamlıca metamorphics were partially transported for a short distance and deposited in paleotrenches which formed on highly fractured, folded, and imbricated serpentinites, during the Middle Miocene. These Middle-Upper Miocene clastic sediments of various size fractions consist mostly of both strongly altered mica schists and minor serpentinites. The altered ash and tephra underlying basalts are observed in some outcrops in the study area, but they are not found in the vicinity of clay quarries. All Taştepe volcanics are amigdaloidal olivine basalt, and the olivines are partially iddingsitizied and serpentinized (Ertürk *et al.*, 1990). This unique clay occurrence is a product of Upper Miocene Taştepe basalts, which ascended through the Ovacık thrust fault, and that cover most of the highly altered mica schists and serpentinites. These materials were transformed to an Fe-smectite series during hydrothermal processes. Representative stratigraphic sections and locations of collected samples are shown in Figure 2.

METHODS OF THE STUDY

The collected samples were washed with deionized water three-four times to dissolve soluble salts that cause flocculation. Excess water was removed by a porcelain filter (0.15 μm pore size) technique under vacuum. Then, the <2-μm size fraction was separated by sedimentation according to Stoke's law. The slurry rested for 7 h 25 min in a glass beaker and then the top ten cm section (<2-μm) was removed by siphoning.

X-ray diffraction (XRD) analysis was performed with a Philips 1140 model X-ray Diffractometer using CuKα radiation, using random-powder mounts and air-dried, oriented clay mineral aggregates, ethylene glycolated, and heated (600°C for 1 h) clay fractions. Li saturation was used to distinguish montmorillonite from beidellite (Greene-Kelly, 1953; Lim and Jackson, 1986). The Greene-Kelly test consists of washing the <2-μm clay samples three times with 1M LiCl and

https://doi.org/10.1346/CCMN.1999.0470301 Published online by Cambridge University Press

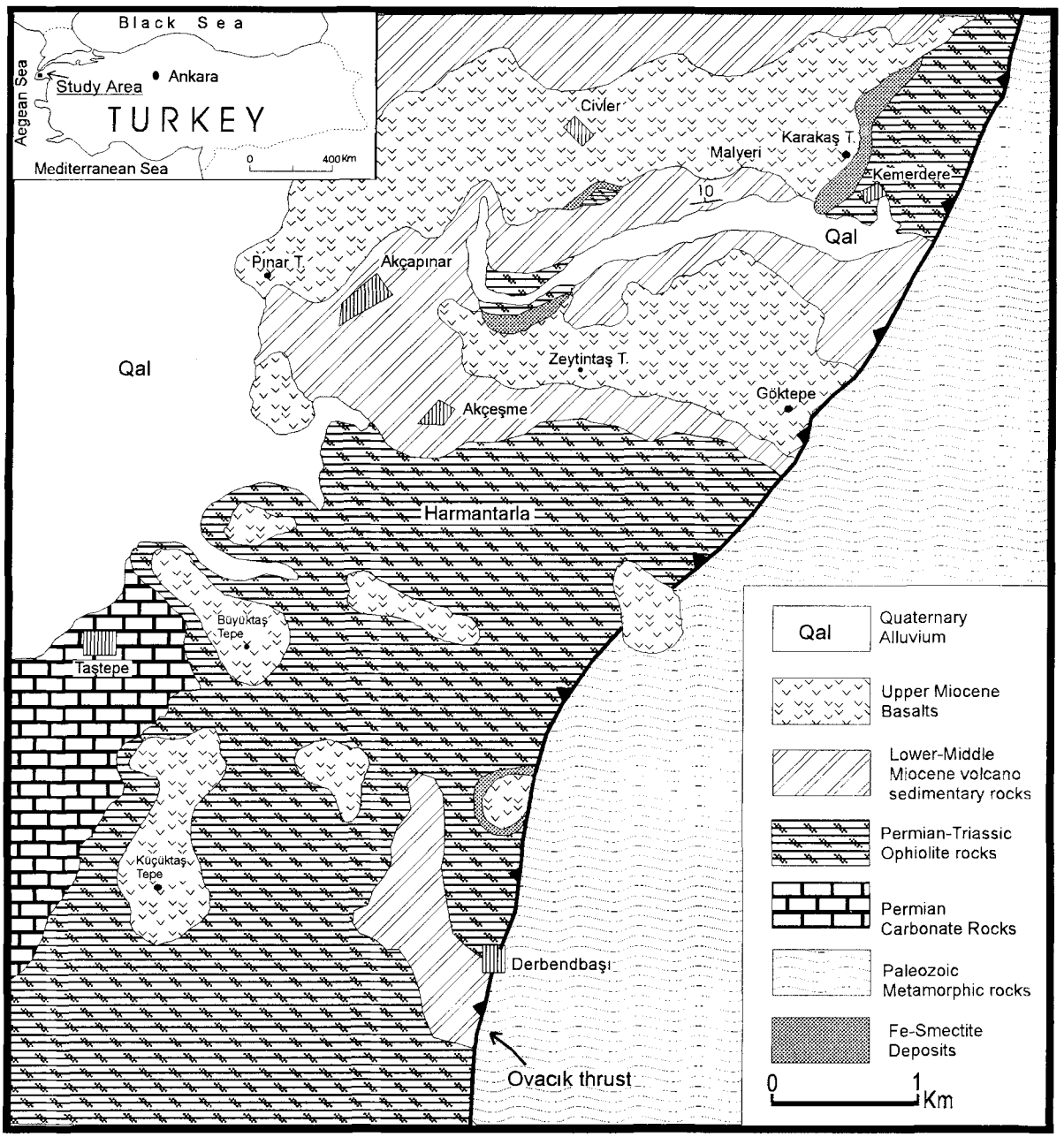

Figure 1. Geological map of the study area.

three times with 80% ethanol in a test tube. The Li-exchanged sample was then collected by centrifuge separation and spread on a pure silica glass slide, heated overnight at 300°C, then placed in a sealed glass container with glycerol and heated overnight in an oven at 90°C (Yamada *et al.*, 1991). If the Li-saturated sample treated with glycerol displays a *d*(001)-value at ~9.6 Å, it indicates a montmorillonite and a spacing of 17.7 Å indicates a beidellite. Clay fractions were saturated (overnight) with K and Mg using 1 mol KCl/liter and 0.5 mol $Mg(OH)_2$/liter, respectively. To distinguish clay minerals, XRD patterns of oriented clay mineral aggregates saturated with K and Mg were obtained after the following treatments: (1) K and Mg saturation with air-dried specimens and (2) K and Mg saturation and ethylene glycol solvation using ethylene glycol vapor at 60°C overnight.

Fourier transform infrared spectroscopy (FTIR) analysis was employed with a JASCO 5300 spectrometer using KBr pellets (200 mg KBr + 0.2 mg sample).

https://doi.org/10.1346/CCMN.1999.0470301 Published online by Cambridge University Press

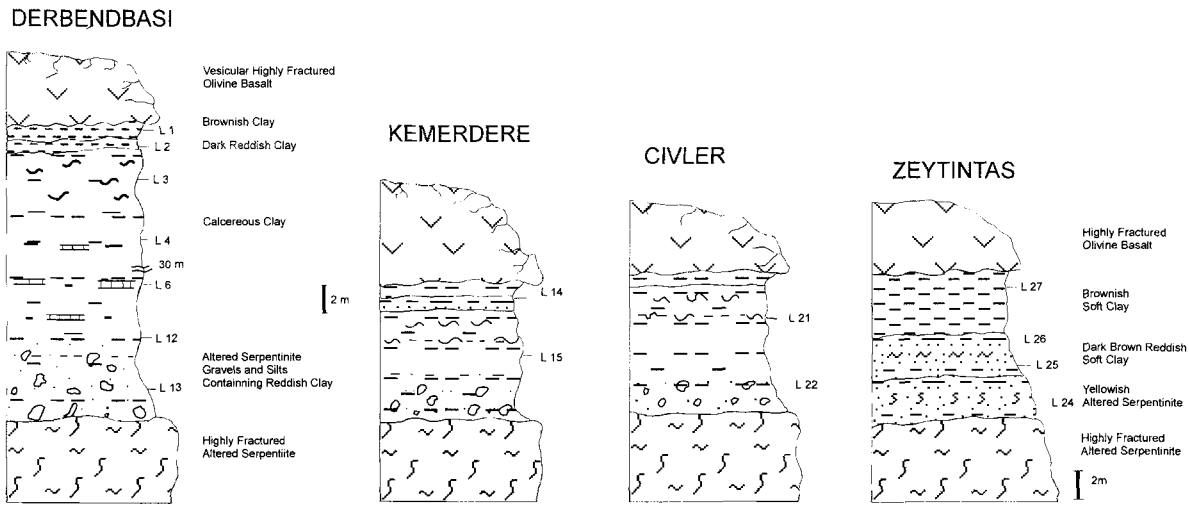

Figure 2. Measured stratigraphic sections in the study area and the locations of samples that were taken.

Small, fresh, broken surfaces of the original undisturbed clay samples were dried at room temperature, coated with Au under vacuum conditions in an Ar atmosphere, and examined by scanning electron microscopy (SEM) (JEOL-SCM-330). Chemical analyses were performed after fusion with Na_2CO_3 in platinum crucibles. Silica was determined gravimetrically, and the other elements with an atomic absorption spectrophometer (AAS) (Perkin-Elmer 3030) after dissolution by HF-$HClO_4$ acid.

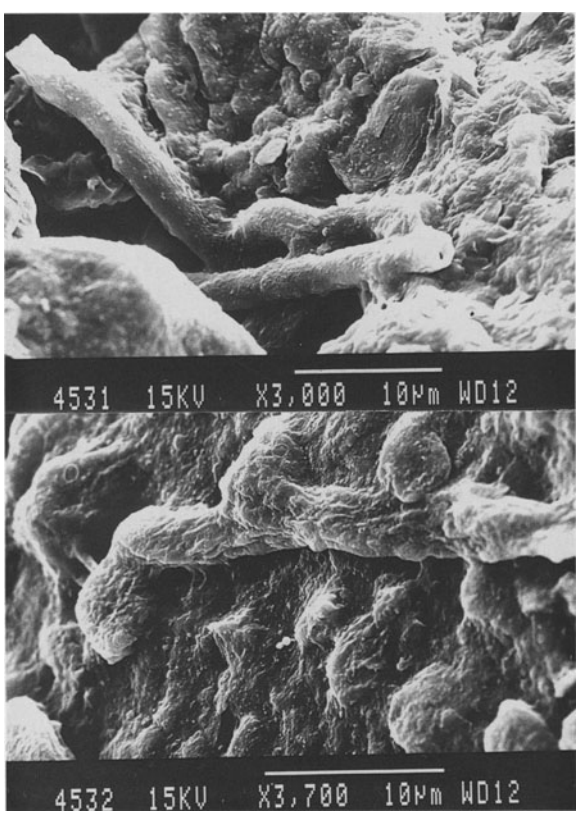

Figure 3. Nontronite occurrence in microtube forms.

RESULTS

SEM studies

The most diagnostic feature of the montmorillonite-nontronite series was micromorphology. In Figure 3, the microtubes are composed of fine and frequently folded clay flakes. The diameter of the microtubes is 2.5–3.0 μm, with wall thickness of 1.0 ± 0.2 μm. The length of the microtubes is 20–30 μm. These microtubes are the result of Fe^{+3} (0.64 Å) substitution for Al^{3+} (0.51 Å), causing interior stretching in the crystal lattice to create microtube morphology with empty space inside. These microtubes consist of several smectite flakes.

In Figure 4, samples show elongated and feathered flakes of intergrown minerals. The most diagnostic micromorphology of nontronites is very thin fibers (4540 in Figure 4), much <0.1 μm in length, arranged parallel in bundles on the edges of the flakes. Similar observations are reported from South Pacific samples based on transmission electron microscopy (TEM) and SEM studies (Singer *et al.*, 1984). According to Mering and Oberlin (1971), nontronite is lath-shaped and has a strong tendency for end-to-end association.

Figure 5 shows development of microporosity as a result of dissolution and precipitation processes with Fe-rich montmorillonite growth forming a honeycomb structure. Figure 6 notably shows sepiolite acicular growth on the edge of highly altered serpentinites. The sepiolite fibers are 0.5–2.0 μm long and <0.05 μm wide. Sepiolite forms as a result of reaction of Si-rich

https://doi.org/10.1346/CCMN.1999.0470301 Published online by Cambridge University Press

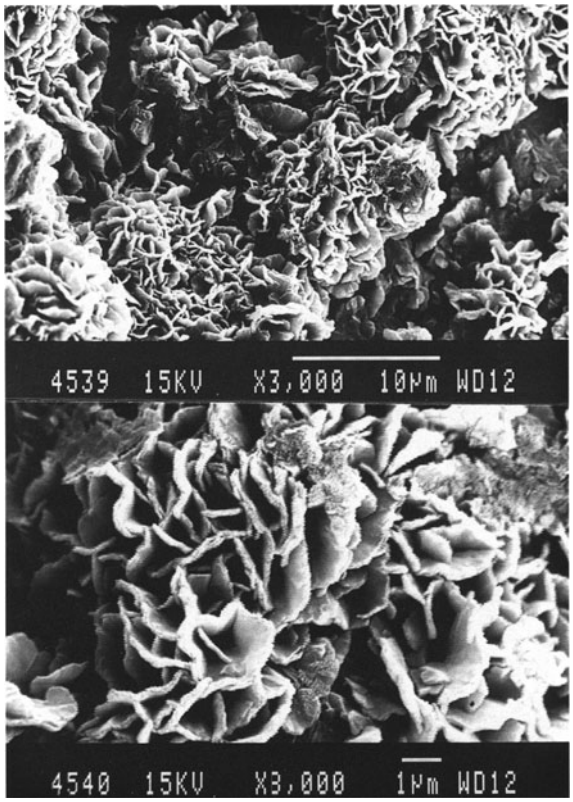

Figure 4. Leaf micro morphology of montmorillonite minerals and occurrence of nontronite fibers are about 0.05 µm in length along the upper edge of montmorillonite. Nontronite occurrence also shown as rosette shape crystal morphology.

hydrothermal solution with highly altered serpentinites at pH ~9 (Ece and Çoban, 1994).

XRD studies

The materials have similar mineralogy consisting of various percentages of dioctahedral smectite, illite, chlorite, talc, calcite, and quartz. Ten representative samples were collected from different stratigraphic horizons to examine the mineralogical composition of the clay fraction. The upper layer of clay occurrence, underlying the basalt layers, contains mainly dioctahedral smectite and minor illite, whereas the lower zone contains very minor amounts of chlorite. Illite concentration decreases downward and illite content doesn't change spatially; it always underlies the basalt layers. It appears that the "crystallinity degree" of dioctahedral smectites increases towards the basalt layer and decreases downward towards serpentinites.

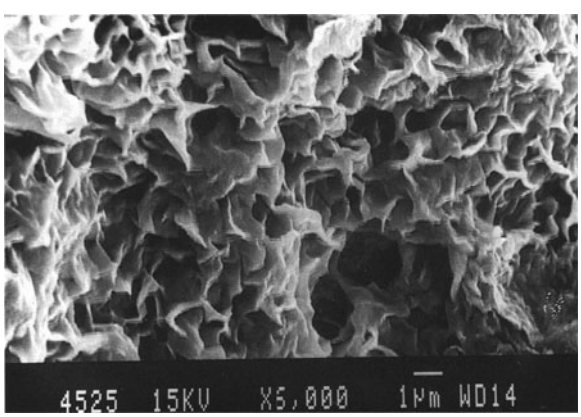

Figure 5. Smectite occurrences formed under the influence of hydrothermal solutions, which were circulated within highly porous and permeable altered rocks.

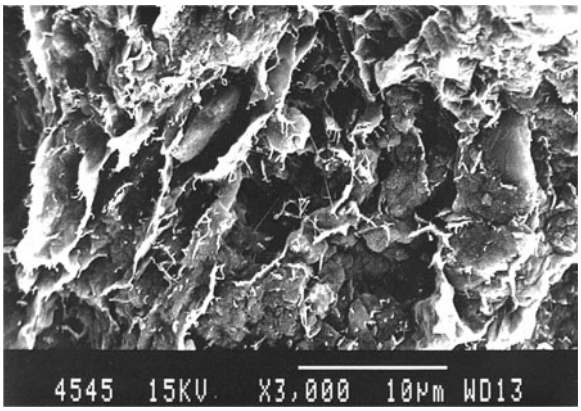

Figure 6. Occurrences of sepiolite fibers 1–2 µm in length along the edges of altered serpentinites.

The air-dried clay fractions of the samples from the brown-dark red 30–50 cm thick zone underneath the basalt (hot contact) layer (L_1, L_7, and L_{14}) exhibit d(001)-values of 14.96, 15.62, and 15.35 Å, which expand to 17.38, 17.13, and 17.56 Å, respectively after saturation with ethylene glycol, and collapse to 9.99, 9.52, and 10.16 Å after heating at 600°C for 1 h. In the brown-dark red zone, illite comprises ~10% of the clay fractions.

In the second dark red clay zone underlying basalt, the <2-µm size fractions of L_2 and L_{27} show that crystallinity degree, mean coherent scattering domains in a particular [001] crystallographic direction, and illite percentage within clay-size fractions decrease downward. Samples L_{13}, L_{22}, and L_{25} from the base level contain minor amounts of chlorite.

Oriented clay mineral aggregates gave very strong basal reflections at 16.66, 15.62, and 14.96 Å for air-dried material and 16.98, 15.49, and 14.59 Å after

Table 1. Summary of d(001) smectite peaks as shown in Figure 7.

Sample no.	Air-dried	KOH	KOH-EG	$Mg(OH)_2$	$Mg(OH)_2$-EG
L_{27}	15.62 Å	14.35	16.05	15.49	16.98
L_7	14.96 Å	12.61	16.50	14.59	16.98
L_{21}	16.66 Å	14.47	17.66	16.98	17.48

https://doi.org/10.1346/CCMN.1999.0470301 Published online by Cambridge University Press

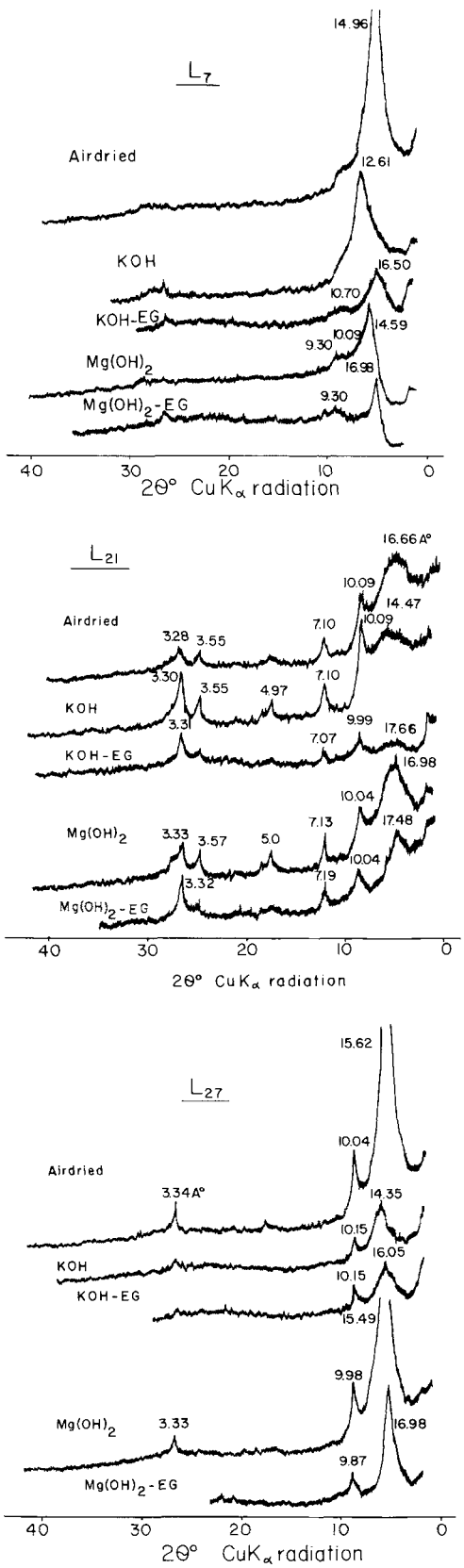

Figure 7. X-Ray diffraction patterns of clay samples. EG = ethylene glycol treated samples after KOH and $Mg(OH)_2$ treatments.

Mg^{2+} saturation (Table 1; Figure 7). Ethylene glycolation of Mg^{2+} saturated samples resulted in full expansion to 17.48 and 16.98 Å. Saturation with K^+ at room humidity (50–60% RH) shifted the *d*(001)-value to 14.47, 14.35, and 12.61 Å, whereas saturation with Mg^{2+} resulted in diffuse reflections at 16.98, 15.49, and 14.59 Å. Upon ethylene glycolation the K^+ saturated samples expanded to 17.66, 16.05, and 16.50 Å (Figure 7). Sample L_7 does not exhibit much expansion after K^+ and Mg^{2+} treatments probably because of a larger nontronite content (15 wt. % Fe_2O_3 in Table 2). Figure 7 (L_{21}) shows that this sample has higher order reflections with a small peak at 7.10 Å, indicating that the main component was smectite and minor chlorite.

Various percentages of calcite are distributed in bulk clay samples. Calcite was derived from dissolution of carbonate blocks located at the thrust boundary and circulation of Ca through the clay deposit by the ground water system. The lack of hematite is probably related to the existence of amorphous iron oxides. Hence, the dark brown color of the clay horizon, 50 cm below the basalt layer, suggests a different iron oxide, whereas the dark-red horizon, 50 cm underneath the dark-brown level, implies changes in iron oxide again.

For the Greene-Kelly Li-test method, samples L_{27}, L_2, and L_{21} were selected to examine the distribution of beidellitic montmorillonitic component throughout the study area. Figure 8 clearly indicates that L_2 contains montmorillonite, and L_{21} shows a small diffraction peak at 17.48 Å, which suggests the presence of a small amount of beidellite. L_{27} shows almost pure montmorillonite at 9.70 Å; L_2 displays a *d*(001)-value at 9.81 Å and a "superlattice effect" at 28.47 Å. The *d*(001)-value of montmorillonite in L_{21} shifts to 9.9 Å due to the presence of a small amount of beidellite in the clay fraction.

IR studies

An intense Si-O stretching absorption band was found at 1023–1039 cm^{-1} (Figure 9). This observation shows agreement of the position of this band in nontronites with Fe^{3+} in tetrahedral sites (Farmer, 1974) and a corresponding band in Fe-montmorillonite at 1035 cm^{-1}. The total iron occupying tetrahedral positions in L_1, L_2, L_3, L_4, and L_6 is consistent with the nontronite-montmorillonite series as determined by chemical analysis. The Si-O stretching absorption at 1028 cm^{-1} and 468 cm^{-1} suggests only minor substitution by Fe^{3+} in the tetrahedral layer. The adsorption

https://doi.org/10.1346/CCMN.1999.0470301 Published online by Cambridge University Press

Table 2. The results of whole rock chemical analyses. Sample locations: L_1, L_2, L_3, L_4, L_6, L_{12} L_{13}, L_{14}, L_{15}, L_{21}, L_{22}, L_{24}, L_{25}, L_{26}, and L_{27} are shown in Figure 2. Iron-rich L_7 and L_8 samples are collected from İzmir highway cuts. L_{11} is from mud cracks in the Derbendbaşı quarry. L_{16}, L_{17}, L_{18}, L_{19} and L_{20} are from the vicinity of Kemerdere village. L.O.I. = loss on ignition.

Sample no.	SiO_2	Al_2O_3	Fe_2O_3	CaO	MgO	SO_3	K_2O	L.O.I.
L_1	70.34	10.33	5.77	3.26	2.47	0.01	1.12	5.4
L_2	70.79	10.98	6.00	3.14	2.55	0.03	1.09	5.40
L_3	67.76	9.82	5.70	5.96	2.27	0.04	1.15	7.71
L_4	70.52	8.89	7.06	2.87	3.33	0.02	0.78	6.83
L_6	70.11	9.55	3.81	6.11	2.03	0.04	1.03	7.29
L_7	47.46	5.98	14.33	3.60	6.79	0.02	0.64	15.66
L_8	48.42	7.46	26.18	1.90	8.84	—	0.26	6.83
L_{11}	46.92	13.94	8.69	8.76	3.72	0.02	1.66	13.90
L_{12}	68.66	10.30	7.34	3.32	2.55	0.02	1.28	5.88
L_{13}	63.91	8.57	5.12	8.43	2.45	0.02	1.10	9.56
L_{14}	74.21	7.70	4.37	5.24	1.90	0.02	1.04	3.69
L_{15}	57.32	6.80	3.93	15.07	1.43	0.02	0.91	13.82
L_{16}	73.04	9.05	4.09	4.96	1.11	0.02	1.21	5.92
L_{17}	44.21	4.68	2.72	23.65	1.28	0.01	0.70	20.98
L_{18}	31.88	4.68	2.85	30.74	1.03	0.02	0.54	27.17
L_{19}	40.46	12.66	9.44	11.41	4.36	0.01	1.38	13.52
L_{20}	39.47	11.76	10.67	11.77	5.24	0.01	0.90	12.20
L_{21}	71.75	9.26	5.71	2.77	1.57	0.01	1.26	5.56
L_{22}	66.46	6.94	7.75	4.18	4.43	0.02	0.88	7.16
L_{24}	43.23	0.41	7.64	8.24	23.07	0.01	0.03	16.75
L_{25}	58.54	8.26	4.55	11.07	1.85	0.01	1.33	11.13
L_{26}	62.11	7.61	4.37	10.42	1.87	0.02	1.21	9.78
L_{27}	69.85	8.95	5.19	3.23	2.01	0.01	0.90	7.32

band at ~780–800 cm^{-1} indicates similar amounts of octahedral Mg^{2+}. The strong adsorption at 3622 and 3405 cm^{-1}, as well as that at 833–835 cm^{-1} is associated with vibrations of the Fe^{3+}, Fe^{3+}-OH stretching. These adsorption bands indicate the Fe occupancy of the octahedral sites. FeFeOH stretching occurs at ~3555 cm^{-1}.

The 3622 cm^{-1} band is a main OH-stretching vibration, with shoulders at 3405 cm^{-1} (Figure 9). AlAlOH and AlMgOH are the predominant groups in the octahedral sheets, so that the 3622 cm^{-1} band must be due to OH-stretching vibrations. The presence of a high Mg content implies that the shoulders at 3405 cm^{-1} must be caused by Fe-OH-Mg and Mg-OH-Mg associations.

A shift toward lower energy with increasing water content was observed in a H_2O stretching mode at 3420 cm^{-1} in Na-montmorillonite (Sposito and Prost,

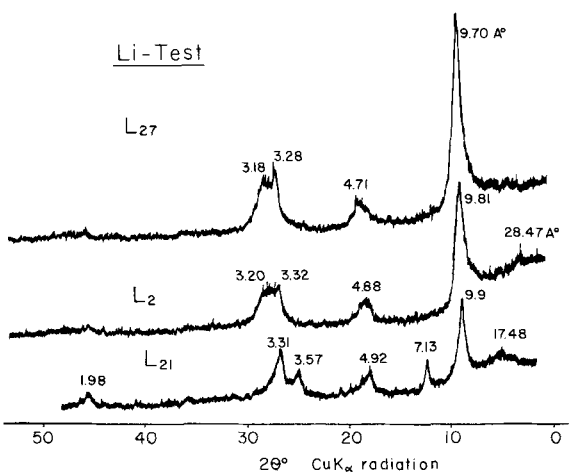

Figure 8. Greene-Kelly Li-test for three samples, indicating the presence of montmorillonite in all samples.

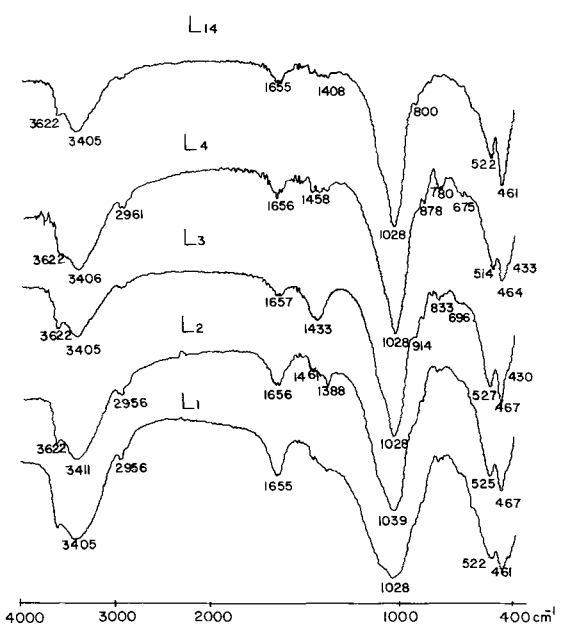

Figure 9. The results of IR spectroscopy analyses.

https://doi.org/10.1346/CCMN.1999.0470301 Published online by Cambridge University Press

Table 3. Chemical analyses of <2-μm size clay fractions. Structural formulae calculations indicate that <2-μm clays contain more than one mineral. Both mixtures of clays and mixed-layer clays are present. L.O.I. = loss on ignition.

Sample no.	SiO_2	Fe_2O_3	Al_2O_3	CaO	MgO	TiO_2	Na_2O	K_2O	L.O.I.
L_1	49.63	9.57	22.07	1.98	3.78	0.53	0.15	2.08	8.69
L_2	50.22	9.79	21.69	2.09	4.02	0.52	0.12	2.09	8.21
L_3	48.51	10.99	21.92	1.98	3.98	0.59	0.23	1.85	8.15
L_4	62.09	8.08	12.75	2.61	4.02	0.63	0.14	1.06	7.98
L_7	52.37	14.66	12.38	0.78	8.80	0.31	0.10	0.64	8.37
$L_{7\text{-}A}$	50.66	15.97	12.84	0.74	8.71	0.39	0.10	0.68	8.42
L_{11}	48.00	10.28	22.81	2.50	3.94	0.76	0.18	2.25	8.90
L_{12}	50.43	11.58	20.00	1.38	3.92	0.62	0.12	2.36	8.72
L_{13}	47.51	9.85	20.77	4.43	3.91	0.64	0.22	1.56	9.91
L_{14}	47.50	7.82	20.05	6.97	5.88	0.43	0.19	1.76	7.90
L_{21}	48.01	11.46	24.39	1.04	3.18	0.60	0.16	2.24	8.46
L_{26}	46.25	10.23	22.36	4.36	4.61	0.46	0.33	1.76	9.53
L_{27}	50.95	9.65	20.95	2.16	4.40	0.60	0.12	1.85	9.07
Tetra-hedron	L_1	L_2	L_3	L_4	L_7	$L_{7\text{-}A}$	L_{11}	L_{12}	L_{13}	L_{14}	L_{21}	L_{26}	L_{27}
Si	3.43	3.54	3.37	3.96	3.64	3.55	3.32	3.48	3.36	3.32	3.30	3.24	3.4
Al	0.57	0.46	0.63	0.04	0.36	0.45	0.68	0.52	0.64	0.68	0.70	0.76	0.5
Octa-hedron	L_1	L_2	L_3	L_4	L_7	$L_{7\text{-}A}$	L_{11}	L_{12}	L_{13}	L_{14}	L_{21}	L_{26}	L_{27}
Al	1.23	1.34	1.16	1.17	0.65	0.61	1.18	1.11	1.09	0.97	1.27	1.08	1.18
Fe	0.50	0.52	0.57	0.39	0.77	0.84	0.53	0.60	0.52	0.41	0.59	0.54	0.50
Mg/2	0.20	0.21	0.21	0.19	0.46	0.46	0.20	0.20	0.21	0.31	0.16	0.24	0.23
Ti	0.03	0.03	0.03	0.03	0.02	0.02	0.04	0.03	0.03	0.02	0.03	0.02	0.03
VI Cat-ions	1.96	2.10	1.97	1.78	1.90	1.93	1.95	1.94	1.85	1.71	2.05	1.88	1.94
Inter-layer	L_1	L_2	L_3	L_4	L_7	$L_{7\text{-}A}$	L_{11}	L_{12}	L_{13}	L_{14}	L_{21}	L_{26}	L_{27}
Mg/2	0.19	0.21	0.20	0.19	0.45	0.45	0.20	0.20	0.20	0.30	0.16	0.24	0.22
Ca × 2	0.30	0.32	0.30	0.36	0.12	0.10	0.36	0.20	0.66	1.04	0.16	0.66	0.32
Na	0.02	0.02	0.03	0.02	0.01	0.01	0.02	0.01	0.03	0.02	0.02	0.04	0.02
K	0.18	0.19	0.16	0.09	0.06	0.06	0.20	0.21	0.14	0.16	0.20	0.16	0.16
Inter-Layer Charge	−0.69	−0.74	−0.69	−0.66	−0.64	−0.62	−0.78	−0.62	−1.03	−1.52	−0.54	−1.10	−0.72

1982). This implies that H-bonding in H_2O for the montmorillonite system increases with increasing water content and that H-bonding is reduced in the interlayer H_2O of dehydrated montmorillonite. Bertie *et al.* (1989) showed also that the intensity of the H_2O stretching vibrations increases with increasing H-bonding.

The 3405 cm^{-1} band is related to the H-O-H stretching vibration of H_2O which is readily lost upon heating. The 3622 cm^{-1} band is related to the fundamental H-O-H stretching vibration and the 1636 cm^{-1} band is related to the H-O-H bending vibration. The infrared absorptions due to structural OH in montmorillonite include the O-H stretching vibration at 3622 cm^{-1} (AlAlOH and AlMgOH bands) and in-plane vibrations at 1028, 915, 878, and 835 cm^{-1} due to $Al_2(OH)$, Fe^{3+}AlOH and MgAlOH (Farmer, 1974). Also the 800 cm^{-1} band is possibly related to Fe^{3+}MgOH. If the distribution of Mg and Fe in the octahedral sheet is random, the Mg-O-Mg absorption should have been very weak and some clustering of Mg ions must be present in the octahedral sheets. IR studies indicate that nontronite has a band at 815 cm^{-1} (FeFeOH). Also, the band at 675 cm^{-1} might belong to nontronite. Calcite appears at 1433 cm^{-1} frequency.

Chemical composition

The major element concentrations of whole rocks are presented in Table 2 and those of the <2-μm size fractions are listed in Table 3. Whole-rock chemical analyses indicate that Na_2O + K_2O is always <2 wt. %, Na_2O content in bulk samples being always <0.5 wt. %, and <0.33 wt. % in clay-size fractions (Ece, unpubl. data). The SiO_2 content increases (~70 wt. %) toward the hot contact zone, which indicates that the clay deposit was under the influence of Si-rich geothermal water rising through the fault zone. However, the SiO_2 content decreases to ordinary values (~50 wt. %) in the <2-μm size fractions (Table 3).

The MgO content increases downward towards the serpentinite and CaO increases in some samples that were collected in the vicinity of the Kemerdere area. Unique Fe_2O_3 rich samples (L_7 and L_{7A}) are from west-end exposures of the basalt layer that is directly un-

https://doi.org/10.1346/CCMN.1999.0470301 Published online by Cambridge University Press

Table 4. Chemical composition of Taştepe basalts (Ertürk *et al.*, 1990).

Sample no.	12	13	17
SiO_2	43.90	61.30	54.0
TiO_2	2.2	0.4	0.6
Fe_2O_3	11.40	2.6	5.60
FeO	3.5	1.80	4.20
MnO	0.1	0.1	0.1
MgO	7.75	0.15	3.20
CaO	9.06	4.05	4.10
K_2O	1.6	3.90	3.0
Na_2O	3.10	3.60	3.0
P_2O_5	0.7	0.1	0.2
Al_2O_3	12.40	14.10	14.0
CO_2	0.66	0.30	2.32
H_2O	0.48	0.60	0.38

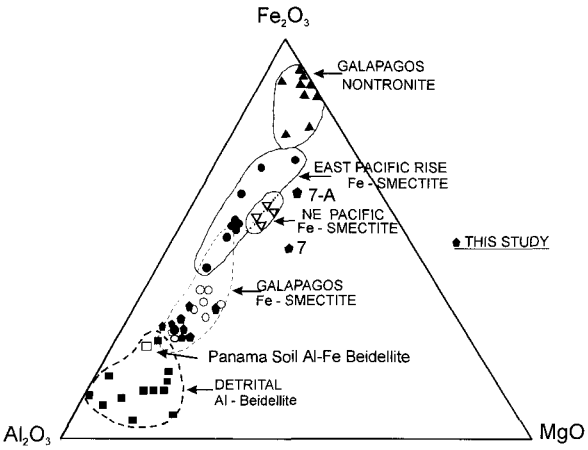

Figure 10. Al_2O_3-Fe_2O_3-MgO diagram for the deep ocean smectites (McMurty *et al.*, 1983).

derlain by serpentinite, and the clay horizon is 10–20 cm thick. It is apparent from the chemical-analyses data that the weathering of mica schists and serpentinites to clay minerals results in a relative enrichment of Si and Al, and a strong depletion of Mg. However, Mg is the predominant exchangeable cation in the soils.

The complete chemical analyses of three Taştepe basalt samples from the study area are given in Table 4 (Ertürk *et al.*, 1990). The Fe_2O_3 contents of the whole-rock clay samples range from 4 to 8 wt. % (Table 2). Samples L_7, L_8, L_{19}, and L_{20} are particularly enriched in Fe. The Fe_2O_3 content significantly increases in clay-size fractions (Table 3) compared to the whole rock (Table 2), suggesting that ferric iron is in octahedral coordination. The above four samples also have high MgO contents, indicating the presence of highly altered serpentinite and chlorite in the clay fraction. A very high MgO content cannot be related only to montmorillonite, and it is more likely that there should be saponite in the clay fractions, in addition to chlorite. The high MgO content of smectites is related to geothermal waters ascending through the underlying serpentinite. All these chemical data indicate that Mg-containing montmorillonite is the main mineral, although L_{21} contains a small amount of beidellite, as shown by the Greene-Kelly test. A summary of chemical analyses of the <2-μm size fractions is shown in Figure 10 for comparison with Fe-rich deep ocean smectites.

The structural formulae are characterized by considerable excess tetrahedral charge. Sample L_4 contains clay-size quartz. The source of Al in the clay minerals is most likely mica schists which are composed mostly of muscovites containing ~30–36 wt. % Al_2O_3. Interlayer charge shows high values (0.62–1.10) depending on ion substitution between tetrahedra. Al is the dominant octahedral cation followed by Fe (0.39–0.84 cations) and Mg (0.19–0.46 cations). Newman and Brown (1987) reported that in all beidellite analyses, Al_2O_3 ranges from 25 to 35 wt. % and Na, K, and Fe concentrations are very low. In contrast, K is ~2 wt. % and Fe_2O_3 ranges between 8–16 wt. % in this study.

We hesitate to give structural formulae of <2-μm size fractions because of mixed clay mineral compositions, as shown in Table 3 and Figure 7. The formula obtained from chemical analyses indicates that (1) the tetrahedral Al^{3+} substituting Si^{4+} is 1.97 and 2.38 which is the limit for normal smectite and chlorite; (2) the total octahedral population is between 2–3 (including total Mg, rather than Mg/2 as shown Table 3), indicating an intermediate di-trioctahedral structure; (3) the octahedral layer is largely occupied by Mg^{2+} and Fe^{3+} and, (4) interlayer Mg^{2+} is absent. Derbendbaşı samples resemble ferric smectite composition in many aspects.

DISCUSSION

The widespread occurrence of ferruginous (Fe^{2+}) beidellites in vertisols suggests that the presence of Fe^{2+}, cyclic oxidizing and reducing conditions, and basic pore solutions promote the crystallization of such clays in Mediterranean and tropical climates (Wilson, 1987). Mack *et al.* (1993) also reported that the formation of an oxisol is the result of extensive alteration of chemically unstable minerals to clay minerals and sesquioxides (oxic horizon). Amorphous iron and aluminum oxides and aluminum-silicon oxides are common in modern oxic horizons, but they are absent from paleosols because of the transformation of the amorphous phases into crystalline phases during diagenesis.

In the study area, the reappearance of talc and chlorite at the base-level indicates the renewal in the influx of Mg-rich hydrothermal solutions. This involves the formation of these minerals by the diagenetic alteration of smectite with an increase of serpentinite-based clay minerals in the lower part of the stratigraphic section. In contrast, illite enrichment in the underlying basalt layer is due to K^+ input during the formation of

https://doi.org/10.1346/CCMN.1999.0470301 Published online by Cambridge University Press

the clay deposit. To transform smectite to illite, the required K^+ came from (1) Si- and K-rich ascending hydrothermal solutions through the fault zone, (2) parent rock which is a mixture of altered mica schists and serpentinites and thereby involving the alteration of mica to illite, and (3) alteration and leaching of K-rich basalts.

Soil developing on serpentinite rocks in the Sierra Nevada and the Coast Range of California contains large quantities of Fe-rich montmorillonite (Wildman *et al.*, 1968a). The clay minerals have a low Mg content relative to Fe, in contrast to the parent serpentinite which has a high Mg content relative to Fe. The Al present in the parent rock (2–8 wt. %) also appears to have been concentrated residually (20–24 wt. %) in the clay minerals. The dissolution of serpentinite minerals under the influence of CO_2-enriched ground waters increases rapidly with an increase in the P_{CO_2}. The rate of Mg dissolution from serpentinite was markedly increased by an increase in the CO_2 content of the solutions in which $P_{CO_2} = 1$ (54–100 ppm; pH = 3.9–4.2) was 25–50 times higher than N_2 atmospheric ($P_{CO_2} = 0$; 1.8–3.5 ppm; pH = 6.7–7.0) conditions. For comparison, pH = 5.3–5.66 at air pressure ($P_{CO_2} = 10^{-3.5}$; 6–12 ppm) (Wildman *et al.*, 1968b). Under such conditions, Mg dissolves more rapidly than Si and much of the Mg leaches out of the soil, explaining the apparent excess of SiO_2 in the clay deposits. The remaining amorphous silica relics slowly dissolve and keep the soil matrix solutions sufficiently high in soluble silica to crystallize Fe-rich montmorillonite. The amounts of Fe and Al, which would be released by the dissolution of adjacent rocks of mica schists and basalts, evidently remain in the soil and become incorporated in the montmorillonite in the Derbendbaşı clay deposits.

By this approach, CO_2-rich geothermal waters, which were circulating through the thrust fault zone, became more important for the formation of Derbendbaşı clay deposits. The increased CO_2 content of ground water would increase the mobility of Mg ions, and possibly explain the apparent excess of SiO_2 in the clay deposits. In contrast, at lower soil water temperatures, the solubility of $Si(OH)_4$ would decrease (~50–80 ppm SiO_2 at O°C compared with 100–140 ppm at 25°C), but the solubility of CO_2 would increase and so would the Mg/Si ratio in the soil matrix solutions (Wildman *et al.*, 1968b).

A high Mg/Si ratio in solution would help to explain the apparent SiO_2 excess in the Fe-rich clays. The solubility characteristics of Mg may explain why Fe-rich montmorillonite was formed in these high Mg soils rather than saponite (Wildman *et al.*, 1968b). According to Wildman *et al.* (1971), the greater stability of the dioctahedral sheet provides a thermodynamic explanation for nucleation of Fe-rich montmorillonite rather than saponite in soils forming on serpentinite rocks, such as the Derbendbaşı clay quarry. The occurrence of high pH, high concentration of Mg and $Si(OH)_4$, and poor drainage develops favorable environments for the formation of saponite. However, in well-drained environments, Fe- and Al-montmorillonites would be stable long before the composition of pore waters approached the stability field of saponite; such an occurrence is rare in nature (Wildman *et al.*, 1968b).

Decarreau *et al.* (1987) studied synthesis and crystallogenesis of ferric smectite in oxidizing conditions and proved that the crystallization of a dioctahedral smectite, containing only Fe^{3+} atoms in the octahedral sheet, is possible under strictly oxidizing conditions. They also found that crystal growth of a ferric smectite is slow. They achieved the synthesis of smectite only at 100–150°C, but even at these temperatures, all particles of the synthetic smectite are not well crystallized. At lower temperatures, only very limited nucleation of clay particles can be detected in the products. Crystal growth cannot be observed in laboratory experiments performed at 25°C. These results suggest crystal growth of the synthetic Fe^{3+}-smectite occurs by transformation of the initial Si-Fe precipitate. Based on these experiments, it is possible to infer that Fe^{3+}-rich smectite forms in the Derbendbaşı clay deposits at very high temperature in a very short time.

CONCLUSIONS

The clay mineral assemblage in all stratigraphic sections in the study area is similar to that of the thickest exposure found in the Derbendbaşı clay quarry. The exposed dark brown-red soils which lie below the basalt layer tend to be differentiated into clay minerals along the thrust fault zone. At the east side, a montmorillonite-beidellite series and an iron-rich variety of chlorite and illite (±talc) predominate and, at the west side, away from the thrust fault zone, a montmorillonite-nontronite series together with Fe-chlorite becomes more abundant. An occurrence of paleosol was covered by hot basalt lavas and no more traces of paleosols are left. No hisingerite, hematite, or sulfide minerals, such as pyrite or sphalerite, were found in this study.

Less than 0.1 μm in length, very thin growths of nontronite fibers were observed on the edges of clay flakes. Diagnostic features of nontronite microtubes are 2.5–3.0 μm in diameter and the lengths of these tubes are ~20–30 μm. Montmorillonite morphology appears as elongated and feathered flakes. Very rare sepiolite occurrences were observed as a product of weathering on the flakes of altered serpentines in micro-environments during SEM studies.

All data showed that the samples consist mostly of montmorillonite, minor beidellite and very minor amounts of vermiculite. XRD data showed, when using the Greene-Kelly Li-test and KOH, $Mg(OH)_2$, and ethylene glycol treatments, heterogeneity in the clay-swelling characteristics, which leads to the conclusion

that the samples may be a mixture of montmorillonite and beidellite with a small amount of nontronite and chlorite (±talc). Chemical data indicated that the smectite minerals are diotahedral in composition with minor trioctahedral minerals.

ACKNOWLEDGMENTS

The authors are indebted to Akçansa Corp. for providing logistic support to complete field work in the summer of 1997. They also express their gratitude to S. Bodur of Kale Bodur Corp. for his help with the chemical analyses. Sincere appreciation is extended to G. Christidis of Technical University of Crete, for his exceptionally careful and productive comments. Also, the authors are grateful to J. Post and S. Guggenheim for their editorial suggestions.

REFERENCES

Badraoui, M. and Bloom, P.R. (1990) Iron-Rich High Charge Beidellite in Vertisols and Mollisols of the High Chaouia Region of Morocco. *Soil Science Society of America Journal*, **54,** 267–274.

Badraoui, M., Bloom, P.R., and Rust, R.H. (1987) Occurrence of High-Charge Beidellite in a Vertic Haplaquoll of Northwestern Minnesota. *Soil Science Society of America Journal*, **51,** 813–818.

Bertie, J.E., Ahmed, M.K., and Eysel, H.H. (1989) Infrared intensities of liquids. 5. Optical and dielectric constants, integrated intensities and dipole moment derivatives of H_2O and D_2O at 22°C. *Journal of Physical Chemistry*, **93,** 2210–2218.

Brigatti, M.F. (1983) Relationships between composition and structure in Fe-rich smectites. *Clay Minerals*, **18,** 177–186.

Christidis, G.E., Scott, P.W., and Marcopoulos, T. (1995) Origin of the bentonite deposits of eastern Milos, Aegean, Greece: Geological, mineralogical and geochemical evidence. *Clays and Clay Minerals*, **43,** 63–77.

Clement, P. and De Kimpe, C.R. (1977) Geomorphological conditions of gabbro weathering at Mount Megantic, Quebec. *Canadian Journal of Earth Science*, **14,** 2262–2273.

Çoban, F. and Ece, Ö.I. (1999) Fe^{3+}-rich montmorillonite-beidellite series in Ayvacık bentonite deposits, Biga peninsula, northwest Turkey. *Clays and Clay Minerals*, **47,** 165–173.

Decarreau, A., Bonnin, D., Badaut-Trauth, D., Couty, R., and Kaiser, P. (1987) Synthesis and crystallogenesis of ferric smectites by evolution of Si-Fe coprecipitates in oxidizing conditions. *Clay Minerals*, **22,** 207–223.

Delvigne, J., Bisdom, E.B.A., Sleeman, J., and Stoops, G. (1979) Olivines, their pseudomorphs and secondary products. *Pedologie*, **29,** 247–309.

Ece, Ö.I. and Çoban, F. (1994) Geology, occurrence and genesis of Eskişehir sepiolites, Turkey. *Clays and Clay Minerals*, **42,** 81–92.

Ercan, T., Satır, M., Steinitz, G., Dora, A., Sarıfakioğlu, C., Adis, C., Walter, J.H., and Yıldırım, T. (1995) Biga yarımadası ile Gökçeada, Bozcaada ve Tavşan adalarındaki (KB Anadolu) tersiyer volkanizmasinin özellikleri. *Maden Tetkik ve Arama Enstatusu Dergisi*, **117,** 55–86.

Ertürk, O., Dinçöz, E., and Alaygut, D. (1990) Petrology of the Cenozoic volcanics in the Biga peninsula, NW Turkey in *International Earth Sciences Congress on Aegean Region Proceedings*, M.Y. Savaşçın and A.H. Eronat, eds., Izmir, Turkey, 368–384.

Farmer, V.C. (1974) *The Infrared Spectra of Minerals*. Mineralogical Society, London, 539 pp.

Greene-Kelly, R (1953) The identification of montmorillonoids in clays. *Journal of Soil Science*, **4,** 233–237.

Kimbara, K. and Honda, S. (1975) An iron-rich saponite-like mineral found in the Moriyama volcanic rocks, Gojome, Akita Prefecture, Japan. *Bulletin of the Geological Society of Japan*, **26,** 37–40.

Kodama, H. and De Kimpe, C.R. (1983) Ferruginous swelling clay minerals in a gabbro saprolite from Mount Megantic, Quebec. *Canadian Journal of Soil Science*, **63,** 143–148.

Kodama, H., De Kimpe, C.R., and Dejou, J. (1988) Ferrian saponite in a gabbro saprolite at Mont Megantic, Quebec. *Clays and Clay Minerals*, **36,** 102–110.

Kohyama, N., Shimoda, S., and Sudo, T. (1973) Iron-rich saponite (ferrous and ferric forms). *Clays and Clay Minerals*, **21,** 229–237.

Lim, C.H. and Jackson, M.L. (1986) Expandable phyllosilicate reactions with lithium on heating. *Clays and Clay Minerals*, **34,** 346–352.

Mack, G.H., James, W.C., and Monger, H.C. (1993) Classification of paleosols. *Geolocial Society of America Bulletin*, **105,** 129–136.

McMurty, G.M., Wang, C.H., and Yeh, H.W. (1983) Chemical and isotopic investigations into the origin of clay minerals from the Galapagos hydrothermal mounds field. *Geochimica and Cosmochimica Acta*, **47,** 475–489.

Mering, J. and Oberlin, A. (1971) The Smectites. In *The Electron-Optical Investigations of Clays*, J.A. Gard, ed., Mineralogical Society, London, 193–230.

Miyamoto, N. (1957) Iron-rich saponite from Maze, Niigata Prefecture, Japan. *Mineralogical Journal*, **2,** 193–195.

Newman, A.C.D. and Brown, G. (1987) The chemical constitution of clays. In *Chemistry of Clays and Clay Minerals*, A.C.D. Newman, ed., Mineralogical Society Monograph 6, London, 1–128.

Okay, A.I., Siyako, M., and Bürkan, K.A. (1990) Biga yarımadası'nın jeolojisi ve tektonik evrimi. (Geology and tectonic evolution of the Biga peninsula) *Bulletin of Turkish Petroleum Geologist*, **2,** 83–121.

Sherman, G.D., Ikawa, H., Uehara, G., and Okazaki, E. (1962) Types of occurrence of nontronite and nontronite-like minerals in soils. *Pacific Science*, **16,** 57–62.

Singer, A., Stoffers, P., Heller-Kallai, L., and Szafranek, D. (1984) Nontronite in a deep-sea core from the South Pacific. *Clays and Clay Minerals*, **32,** 375–383.

Siyako, M., Bürkan, K.A., and Okay, A.I. (1989) Biga ve Gelibolu yarımadalarının tersiyer jeolojisi ve hidrokarbon olanakları (Tersiyer geology and hydrocarbon potential of the Biga and Gelibolu peninsulas) *Bulletin of Turkish Petroleum Geologist*, **1,** 183–199.

Sposito, G. and Prost, R. (1982) Structure of water adsorbed on smectites. *Chemical Reviews*, **82,** 553–573.

Wildman, W.E., Jackson, M.L., and Whittig, L.D. (1968a) Iron-rich montmorillonite formation in soils derived from serpentinite. *Soil Science Society of America Proceedings*, **32,** 787–794.

Wildman, W.E., Jackson, M.L., and Whittig, L.D. (1968b) Serpentinite rock dissolution as a function of carbon dioxide pressure in aqueous solution. *American Mineralogist*, **53,** 1252–1263.

Wildman, W.E., Whittig, L.D., and Jackson, M.L. (1971) Serpentinite stability in relation to formation of Fe-rich montmorillonite in some California soils. *American Mineralogist*, **56,** 587–602.

Wilson, M.J. (1987) Soil smectites and related interstratified minerals: Recent developments. In *Proceedings of the International Clay Conference, 1985, Denver*, L.G. Schultz, H. van Olphen, and E.A. Mumpton, eds., Clay Mineral Society, Bloomington, Indiana, 167–173.

Yamada, H., Nakazawa, H., Yoshioka, K., and Fujita, T. (1991) Smectites in the montmorillonite-beidellite series. *Clay Minerals*, **26,** 359–369.

(*Received 5 June 1998; accepted 7 September 1998; Ms. 98-072*)